Fuel Processing Technology 126 (2014) 95–103

Contents lists available at ScienceDirect

Fuel Processing Technology

journal homepage: www.elsevier.com/locate/fuproc

Preparation of activated carbon-metal oxide hybrid catalysts: textural characterization

A. Barroso-Bogeat, M. Alexandre-Franco, C. Fernández-González, V. Gómez-Serrano *

Department of Organic and Inorganic Chemistry, Faculty of Sciences, University of Extremadura, Avda. de Elvas s/n, E-06006 Badajoz, Spain

ARTICLE INFO

Article history:
Received 20 February 2014
Received in revised form 10 April 2014
Accepted 17 April 2014
Available online 10 May 2014

Keywords:
Activated carbon
Metal oxides
Hybrid catalysts
Textural characterization

ABSTRACT

In catalysis processes, activated carbon (AC) and metal oxides (MOs) are used as catalysts and catalyst supports because of their textural and chemical properties. A combination of AC and MO properties in a single catalyst entails changes in the catalytic activity and behaviour which would redound to the number of applications. The present study aims at preparing AC-MO hybrid catalysts by chemical interaction of MO precursors in aqueous medium with AC and at carrying out the textural characterization of the samples. From a commercial AC and six MO precursors (i.e. Fe^{3+}, Al^{3+}, Zn^{2+}, $SnCl_2$, TiO_2, and WO_4^{2-}), three series of hybrid catalysts were prepared by wet impregnation and oven-drying at 120 °C and subsequent heat treatment of the resulting products at 200 or 850 °C in inert atmosphere. The samples were characterized texturally by N_2 adsorption at −196 °C, mercury porosimetry, and density measurements. Therefore, the influence of the MO precursor and heating conditions on the porous texture is studied. Yield varies more widely for the samples prepared at 120 °C and 850 °C than at 200 °C. The mass increase after oven-drying at 120 °C and the mass decrease after heating at 850 °C are much greater for the Sn catalysts. Because of the support of MO precursors on AC, in general, macro-, meso-, and microporosity significantly decrease. The effects on the texture of AC are by far more important for the Sn catalyst and also, though less, for the Fe catalyst. However, they are weaker for the W and Ti catalysts. In general, the heat treatment at 200 °C only causes small changes in the porous texture of the samples. By heating at 850 °C the pore size distribution becomes more uniform in the three porosity regions. Microporosity develops chiefly for the Sn catalyst, whereas mesoporosity does mainly for the Sn and Fe catalysts. The textural modifications have been associated with mass, composition, and structural modifications.

1. Introduction

Activated carbon (AC) is used as a catalyst on its own and much more frequently as a support for catalysts [1–6]. ACs are used as catalyst supports because, as unique virtues, they gather the possibility to tailor the physical surface properties and to modify the chemical surface properties and the nature of the interaction with the catalyst, and others [2,5]. Metal oxides (MOs) represent one of the most important and widely employed categories of solid catalysts. As AC, they may also be used either as the active phase or as the support. Among the MO catalysts, those of transition metals occupy a predominant place owing to their low-production cost, easy regeneration, and selective action. MOs are utilized both for their acid–base and red-ox properties [7–9]. In the last decade, however, there has been a growing interest in the synthesis and applications of mixed MOs [10,11]. From carbon molecular sieves, composite catalysts constituted by inorganic oxides dispersed in a carbon matrix have also been prepared [12]. AC-supported metal oxide catalysts have been used for a great variety of chemical reactions, i.e. Fe_2O_3, ZnO and TiO_2, degradation of organic compounds [13–20]; Fe_2O_3, hydroxylation of benzene [21,22], dehydrogenation of propane [23], acylation of alcohols and amines [24], and so forth; WO_3, decomposition of isopropanol [25,26], isomerization of 1-butene [27], decomposition of methanol and ethanol [28], combustion of toluene [29], hydrogenation of ethylene [30]; SnO_2, low temperature oxidation of CO [31,32], AC-covered Al_2O_3, hydroprocessing and hydrodesulfurization processes [33,34].

The use of AC as support for catalysts is mainly based on its porous structure and surface functional groups. The porous structure controls the availability of surface active sites and thereby the degree of catalyst dispersion. In catalysis processes, the dispersion of the catalyst plays a key role as it enhances its efficiency. To achieve a high degree of catalyst dispersion, ACs are often used because of their high surface area. Another important factor in such processes is the pore size distribution of AC. ACs are characterized by a very broad pore size distribution ranging from molecular dimension to several hundred nanometers. Depending on the size of the reactant and of the product molecules, the catalyst dispersed in small pores would be more or less effective. Therefore, the pore size distribution is an important consideration when selecting the appropriate carbon to use as a support [35], minimizing diffusion

* Corresponding author. Tel.: +34 924 289421; fax: +34 924 271449.
E-mail address: vgomez@unex.es (V. Gómez-Serrano).

http://dx.doi.org/10.1016/j.fuproc.2014.04.022
0378-3820/

limitations and catalyst deactivation [36]. Typical ACs are essentially microporous materials and therefore may be texturally sensitive to the support of catalysts on their surface. On the other hand, textural properties such as surface area and porosity have a remarkable impact not only on the catalyst dispersion but also on the reduction of metal chemical species on the surface of AC, especially when the conventional incipient wetness impregnation technique is used in the preparation of the catalysts ([37] and references therein). The surface functional groups, especially oxygen complexes, present on the carbon support can provide anchorage sites for the catalyst precursor and act as active centres in multifunctional catalysts due to their acid–base or red-ox properties [38,39]. In addition to act as nucleation anchors, it has also been reported that the surface groups can improve the access of metal solutions because of the decrease in the hydrophobicity of the carbon [37].

In view of the numerous reactions catalyzed by AC-MO catalysts and of the essential role played by the porous structure not only in the preparation of these hybrid catalysts but also in their subsequent use in catalysis processes, the focus of the present study was on the preparation and textural characterization of AC-MO hybrid catalysts. In these catalysts, it can be regarded AC as a MO support which may further behave at the same time as an active catalyst. Of course, the hybrid catalysts are susceptible to be used in the same catalysis reactions (i.e. with reactant in gas or liquid phase; red-ox, acid–base, etc.) as AC and MOs separately, being then possible to diversify the applications of such catalysts as compared to their AC and MO parents. The catalytic activity for the hybrid catalysts will be determined not only by the specific activities of AC and MOs but also by their contents in the samples. In best a synergistic effect may occur for the hybrid catalysts.

Using a commercial AC and the wide series of MO precursors, AC-MO hybrid catalysts are prepared and characterized texturally. Since catalysis processes of industrial interest need to heat at relatively high temperatures [4], at which physico-chemical properties of the catalyst may undergo modifications and thereby influence the catalytic behaviour, three series of hybrid catalysts are prepared by heating under different conditions. The resulting samples are characterized in terms of porous structure by gas adsorption at low temperature, mercury porosimetry, and density measurements.

2. Experimental

2.1. Materials and reagents

A granular AC from Merck® (Darmstadt, Germany), 1.5 mm average particle size (Cod. 1.02514.1000), as received, was used as MO support. For AC, the ash content is 4.72 wt.%, which is markedly lower than for other activated carbons that may contain up to 15 wt.% of mineral matter (the nature and amount are a function of the precursor) [4]. Ashes are composed of mullite and SiO_2. The elemental composition (wt.%) is: C, 86.5; H, 0.51; N, 0.26; S, 0.64; O, 7.37. pH of the point of zero charge is 10.50. Metal nitrates, which are readily soluble in water, as a rule were used as MO precursors. These were $Al(NO_3)_3{\cdot}9H_2O$, $Fe(NO_3)_3{\cdot}9H_2O$, $SnCl_2{\cdot}2H_2O$, $Na_2WO_4{\cdot}2H_2O$ and $Zn(NO_3)_2{\cdot}6H_2O$, all of them purchased from Panreac® (Barcelona, Spain) and being of reagent grade. As an exception to the rule, anatase powder (Aldrich®; Steinheim, Germany) was used as TiO_2 precursor.

2.2. Preparation of hybrid catalysts

Most hybrid catalysts were prepared by the well-known method of wet impregnation [40]. Around 25 g of AC were impregnated with 250 mL of an aqueous solution of the corresponding MO precursor, using a precursor to AC ratio of 1:1. The impregnation system was placed in a three necked flask and heated at 80 °C under continuous mechanical agitation of 100 rpm for 5 h. Once this time had elapsed, the impregnated products were first vacuum-filtered with aid of a water pump and then oven-dried at 120 °C for 24 h.

The AC-TiO_2 hybrid catalyst was prepared by slightly modifying the method of impregnation at high temperature previously proposed by Kahn [41,42]. In such a method, 25 g of AC were impregnated with 250 mL of an aqueous suspension containing 1.25 g of anatase powder, by heating also at 80 °C for 5 h under continuous stirring of 300 rpm. Then, after vacuum-filtration, the resulting solid in two successive steps was thoroughly washed with deionised water until total colour loss in the residual liquid and oven-dried at 120 °C for 24 h. Anatase was selected as the catalyst precursor because the photocatalytic activity of TiO_2 seems to be mainly associated with the anatase-type structure [43].

Subsequently, the oven-dried products were calcined at 200 or 850 °C in a horizontal cylindrical furnace. About 2 g of product were weighed in an analytical balance, placed in a small steel container, and heated from room temperature up to the calcination temperature in an inert atmosphere of high purity (i.e. >99.998 vol.%) nitrogen (flow rate = 100 mL·min^{-1}). The heating rate was 10 °C·min^{-1}. The holding time at maximum heat treatment temperature was 2 h. Next, the system was allowed to cool down to room temperature under the same flow of nitrogen. These experiments were carried out in duplicate or in triplicate in order to obtain the required mass of each catalyst for later studies. For comparison purposes, two samples were obtained by heating only AC, in the absence of any metal oxide, under the same conditions as in the preparation of the hybrid catalysts.

The yield of the process of preparation of the catalyst samples was calculated as (M_f/M_i) x 100, with M_i being the mass either of AC (i.e. 25 g) used in the impregnation treatment or of the samples of series 1 used in the subsequent heat treatment, whereas M_f is the mass of final product after oven-drying at 120 °C or heat-treating at 200 or 850 °C. As a whole, three series of catalyst samples were prepared, i.e. three of these samples with each MO, depending on heating conditions in the oven-drying and calcination treatments. They are: series 1: 120 °C, 24 h; series 2: 200 °C, 2 h; series 3: 850 °C, 2 h. The codes assigned to the catalysts are shown in Table 1. The samples prepared from AC are referred to in the text as AC200 and AC850.

2.3. Textural characterization study

The textural characterization of the samples was accomplished by gas adsorption (N_2 at −196 °C), mercury porosimetry, and helium and mercury density measurements. The N_2 adsorption isotherms were determined using a semiautomatic adsorption apparatus (Autosorb 1), Quantachrome®. About 0.10 g of sample was first oven-dried at 110 °C overnight and then out-gassed at 120 °C for 12 h, at a pressure lower than 10^{-3} Torr, prior to starting adsorption measurements under equilibrium conditions. The out-gassing temperature was selected in accord with the temperature of preparation of the catalyst samples of series 1. The N_2 isotherm provides valuable information on the pore size distribution in the regions of micro- and mesopores (i.e. macropores are not amenable to the gas-adsorption analysis), surface area, and pore volumes. In relation to the various porosity regions it is relevant to point out that a widely accepted classification of the pores by their average width (w) is: micropores, w < ~20 Å; mesopores, ~ 20 Å <w < ~500 Å, and macropores (w > ~500 Å) [44]. The pore size distribution in the

Table 1
Preparation of the metal oxide-AC catalysts. Sample codes.

Precursor	Heat treatment temperature		
	120 °C	200 °C	850 °C
$Al(NO_3)_3{\cdot}9H_2O$	A120	A200	A850
$Fe(NO_3)_3{\cdot}9H_2O$	F120	F200	F850
$SnCl_2{\cdot}2H_2O$	S120	S200	S850
TiO_2 anatase	T120	T200	T850
$Na_2WO_4{\cdot}2H_2O$	W120	W200	W850
$Zn(NO_3)_2{\cdot}6H_2O$	Z120	Z200	Z850

micropore range was calculated by the Horvath-Kawazoe (H-K) method [45]. The theoretical background for microporosity characterization was based on Dubinin's theory. Thus, the analysis of the adsorption isotherms by Dubinin-Radushkevich (D-R) equation led to the micropore volume, W_0 [46]. From the characteristic energy E_0 ($kJ \cdot mol^{-1}$), as obtained also from the slope of the D-R plot, the average micropore width (L_0, nm) was calculated [47]. The apparent surface area (S_{BET}) was estimated by means of the Brunauer, Emmett and Teller (BET) equation [48]. The D-R equation and BET equation as a rule were applied in the P/P^0 ranges between 6.7 x 10^{-4} and 7 x 10^{-2} and between 0.05 and 0.35, respectively. The linear regression coefficient (R^2) was higher than 0.999 for the D-R equation and than 0.99 for the BET equation.

Mercury porosimetry enables to characterize the macro- and mesopore structures of porous solids. Mercury intrusion experiments were carried out in a mercury porosimeter (PoreMaster-60), Quantachrome®. The computational program of the porosimeter used the values of surface tension and contact angle of 0.480 $N \cdot m^{-1}$ and 140°, respectively. In mercury porosimetry, the volume of mercury taken up by the solid is measured as the applied pressure is gradually increased. The pore size distribution curves are obtained by differentiation of the curves of cumulative volume (V_{cu}) against pore radius (r) [44]. From the latter curves, macropore (V_{ma}) and mesopore (V_{me}) volumes were obtained as follows:

$$V_{ma} = V_{cu}(r = 250\ Å) \quad (1)$$

$$V_{me} = V_{cu}(r < 20Å) - V_{ma} \quad (2)$$

Mercury density (ρ_{Hg}) was measured just before starting the mercury porosimetry experiment. About 0.3 g of sample was evacuated until the pressure of 1.333 Pa was reached in the porosimeter. Helium density (ρ_{He}) was determined in a Quantachrome® steropycnometer, using around 3 g of sample. From ρ_{Hg} and ρ_{He}, the total pore volume (V_T) was calculated by applying the expression (3) [49]:

$$V_T = \frac{1}{\rho_{Hg}} - \frac{1}{\rho_{He}} \quad (3)$$

For comparison purposes, the total pore volume (V'_T) was also estimated from W_0, V_{me} and V_{ma} by the following expression:

$$V'_T = W_0 + V_{me} + V_{ma} \quad (4)$$

3. Results and discussion

3.1. AC and AC samples

The N_2 adsorption isotherms measured for AC, AC200 and AC850 are plotted together in Fig. 1(a), for comparison purposes. Such isotherms by their shape closely resemble type I isotherm of the well-known BDDT classification system [50] and therefore AC and both AC-derived samples are mainly microporous solids. Furthermore, the steady but non-regular increase of the N_2 adsorption with the gradual rise of P/P^0 between 0.0 and 1.0 indicates that the carbon samples possess a very broad pore size distribution in the regions of micro- and mesopores, with predominance of narrow and wide pores, respectively [51]. Moreover, the large adsorption of N_2 at very low P/P^0 values (see the great slope of the ascending branch at $P/P^0 \approx 0.0$ in the adsorption isotherms) proves a great presence of narrow microporosity in the samples. Finally, the open knees of the adsorption isotherms at higher P/P^0 indicate that wider micropores of varying size are present in the samples.

The three maxima shown by the H-K plots in Fig. 1(b) at 8, 10–12 and 14 Å pore diameters denote that the porosity distribution is three-modal in the samples. From peak intensities it follows that micropores

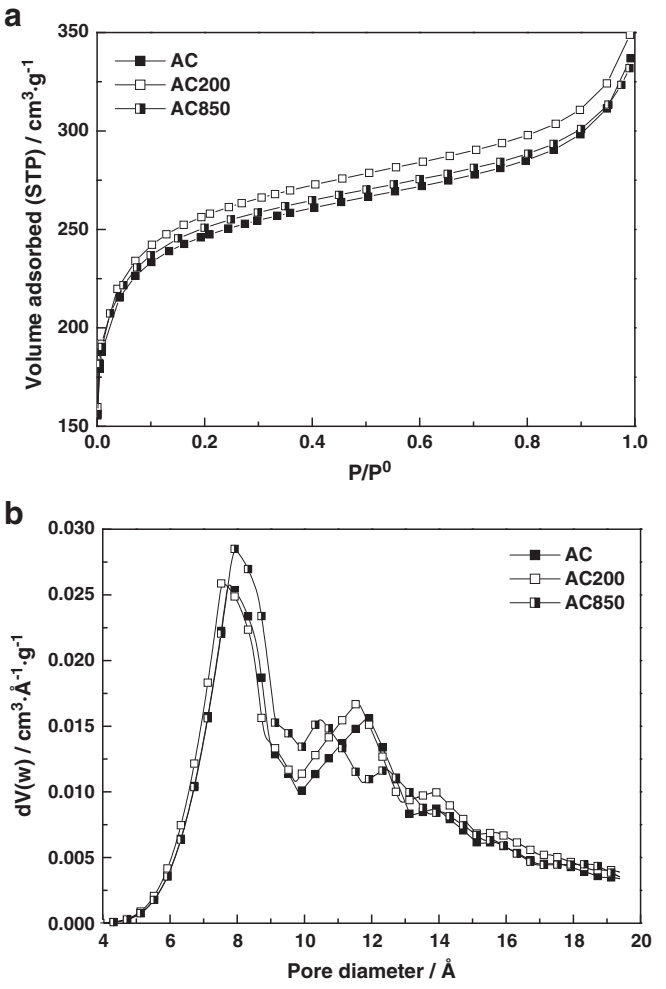

Fig. 1. N_2 adsorption isotherms at −196 °C (a) and micropore size distributions (b) of AC and heat-treated AC samples.

are less abundant as the pore size increases. Also notice that the smallest size micropores undergo a slight widening when heating at 850 °C, whereas the intermediate size micropores narrow with increasing heat treatment temperature above 120 °C. These heat treatment temperature-dependent effects on the microporous structure of AC are attributable to the occurrence of mass loss and pore shrinkage. The yield of the process of preparation of AC200 and AC850 is 97 and 95 wt.%, respectively. Therefore, it is probable that the mass loss is mainly due to the removal of hydration water for AC200 and not only to dehydration but also to the removal of carbon-oxygen surface functional groups for AC850. The presence of hygroscopic water and of oxygen surface groups in AC can be accounted for by the high adsorption capacity and tendency to oxidation exhibited commonly by AC. A microporosity decrease at high heat treatment temperature has been frequently reported elsewhere [52–54] and connected with lateral growth and increase in planarity of layer planes [55]. However, the L_0 values in Table 2 show that the average size of the micropores remains practically unaltered after the heat treatment of AC at 200 or 850 °C. It also applies to the micropore volume (see the W_0 values in Table 2), which is in line with the area under the H-K curves in Fig. 1(b).

As far as mesoporosity is concerned, Fig. 1(a) also shows a slight adsorption increase in the P/P^0 range from 0.1–0.2 to 0.8–0.9 and a much more pronounced slope increase at higher P/P^0 values. Accordingly, it becomes apparent that mesoporosity is heterogeneous in the analyzed samples, with the mesopores of larger sizes being predominant. A heterogeneous porosity not only in the region of mesopores but also in the region of macropores is also shown by the curves of mercury

Table 2
Textural data for AC and heat-treated AC samples.

Sample	S_{BET} ($m^2 \cdot g^{-1}$)	W_0 ($cm^3 \cdot g^{-1}$)	L_0 (nm)	V_{me} ($cm^3 \cdot g^{-1}$)	V_{ma} ($cm^3 \cdot g^{-1}$)	V_T' ($cm^3 \cdot g^{-1}$)	ρ_{He} ($g \cdot cm^{-3}$)	ρ_{Hg} ($g \cdot cm^{-3}$)	V_T ($cm^3 \cdot g^{-1}$)
AC	711	0.36	1.00	0.15	0.21	0.72	2.03	0.89	0.63
AC200	745	0.37	1.00	0.14	0.18	0.69	2.03	0.94	0.57
AC850	746	0.37	1.00	0.14	0.20	0.71	2.01	0.75	0.83

intrusion in Fig. 2(a). Thus, the cumulative pore volume varies almost linearly with pore radius. Furthermore, the derivative curves in Fig. 2(b) feature a great slope branch at pore radii smaller than 40 Å and three maxima centred at 80, 250 and 2500 Å. Notice that peak intensities are somewhat lower for AC200 and AC850 than for AC, which indicates surprisingly that the heat treatment of AC at 200 and 850 °C caused slight meso- and macroporosity reductions.

From the obtained W_0, V_{me} and V_{ma} values (data in Table 2) it becomes apparent that the pore structure is tri-disperse in AC, AC200, and AC850. The pore volumes in the three ranges of pore sizes are in line with those for typical activated carbons [56]. As expected, W_0 is higher than V_{me} and V_{ma}. In fact, W_0 is equal to V_{me} plus V_{ma}. Furthermore, V_{ma} is markedly higher than V_{me}. Moreover, W_0 is only slightly higher for AC200 and AC850 than for AC. However, V_{ma} and V_{me} are somewhat lower for the couple of heat-treated samples. As a guide, the pore volumes vary by 14% for V_{ma} at most. Also, V_T' is rather similar for the three carbon samples. Therefore, the heat treatment of AC at 200 or 850 °C does not result in significant changes in the pore volumes, as measured by N_2 adsorption and mercury porosimetry. However, V_T is 0.63 $cm^3 \cdot g^{-1}$ for AC and varies widely between 0.57 $cm^3 \cdot g^{-1}$ for AC200 and 0.83 $g \cdot cm^3$ for AC850. In view of the ρ_{He} and ρ_{Hg} values listed in Table 2, the opposite variation of V_T for AC200 and AC850 seems to arise from ρ_{Hg} rather than from ρ_{He}. If so, the porosity decrease and increase for AC200 and AC850, respectively, would concern porosity made up of smaller pores than the molecule of gas helium with a diameter of approx. 2.3 Å [56]. Finally, it should be mentioned that the S_{BET} values in Table 2 indicate that the carbon samples possess a well-developed surface area, which is slightly increased for AC200 and AC850 as compared to AC.

In brief, the textural modifications originated as a result of the heat treatment of AC at 200 or 850 °C are of little significance. Therefore, the textural changes produced in the preparation of the hybrid catalysts, if any, will be mainly due to the chemical and heat treatments effected in the preparation of the hybrid catalyst samples.

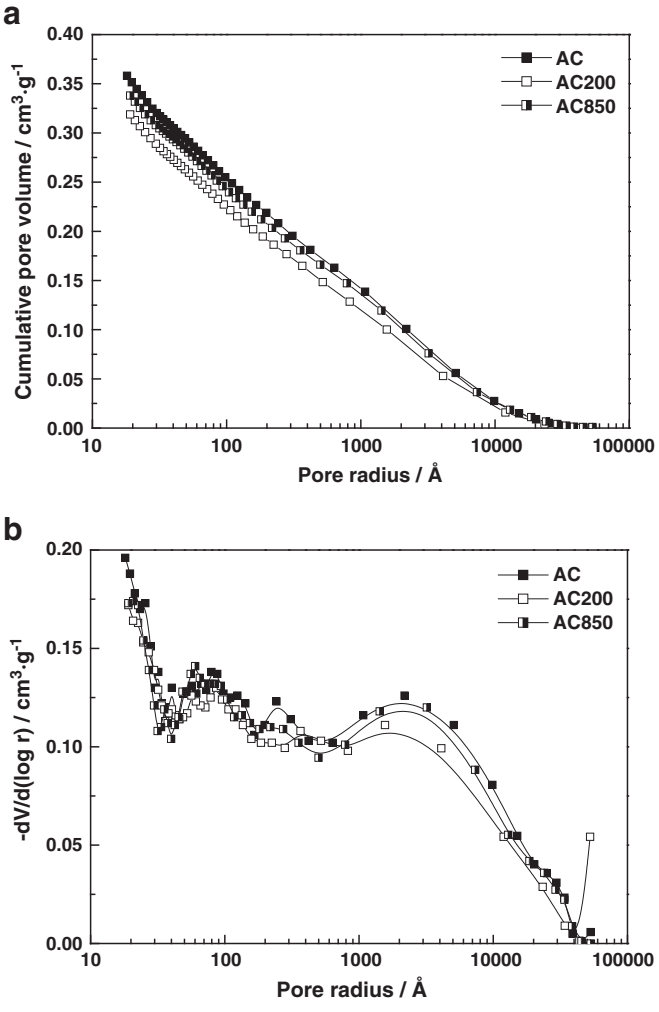

Fig. 2. Cumulative pore volume versus pore radius (a) and meso- and macropore size distributions (b) of AC and heat-treated AC samples.

3.2. Series 1

For the hybrid catalysts of series 1, yield (data in Table 3) varies by S120 ≫ F120 > W120 > T120 ≈ Z120 > A120 and in the very wide range between 149 wt.% for S120 and 102 wt.% for A120. Furthermore, it is relatively high for F120 and, though less, for W120. For A120, T120 and Z120, yield presents close values and is only slightly above 100 wt.%. The N_2 adsorption isotherms in Fig. 3(a), in general, are very similarly shaped to the isotherm measured for AC in Fig. 1(a). Therefore, the impregnation of AC with the MO precursors containing aqueous systems and subsequent oven-drying at 120 °C as a rule does not bring about strong changes in the micro- and mesopore size distributions of AC. As the only different features, the isotherms of AC and hybrid catalysts clearly show that the adsorption of N_2 at very low P/P^0 is significantly lower for a large number of samples (i.e. W120, A120, Z120 and F120) and that it decreases drastically over the P/P^0 range for S120. Conversely, adsorption slightly increases above $P/P_0 \approx 0.1$ for T120. Accordingly, it seems first that the support of most of the MO precursors on AC produces a significant micropore blockage and as a last resort porosity closing for most of the catalyst samples. The relative position of the adsorption isotherms in Fig. 3(a) indicates that the effect of microporosity loss varies by F120 > Z120 ≈ A120 > W120. Second, such an effect is much stronger and embraces not only micropores but also mesopores for S120. Third, the incorporation of TiO_2 (anatase, powder) to the AC support gives rise to the creation of a small fraction of mesopores, without affecting the measurable microporosity.

The micropore size distributions for selected samples of series 1, as calculated by means of the H-K method, are shown in Fig. 3(b). As expected, it is by far different only for S120, as shown by the absence of the peaks at 14 and 10–12 Å from the S120 plot and also by the weaker peak at 8 Å in such a plot than in the AC plot. From the curves of mercury intrusion in Fig. 4(a) and their derivative curves in Fig. 4(b) it is also evident that for S120 a great mesoporosity decrease occurs, mainly concerning narrow and wide mesopores. Notice that the maximum at 225 Å in the AC curve is completely missing not only from the S120 curve but also from the F120 and T120 curves, which proves that wide mesopores are also absent from F120 and T120. Macroporosity undergoes a marked decrease for S120 and F120, the effect of porosity loss being much weaker for the rest of the samples.

Table 3
Textural data for catalysts of series 1.

Catalyst	Yield (wt.%)	S_{BET} ($m^2 \cdot g^{-1}$)	W_0 ($cm^3 \cdot g^{-1}$)	L_0 (nm)	V_{me} ($cm^3 \cdot g^{-1}$)	V_{ma} ($cm^3 \cdot g^{-1}$)	V_T' ($cm^3 \cdot g^{-1}$)	ρ_{He} ($g \cdot cm^{-3}$)	ρ_{Hg} ($g \cdot cm^{-3}$)	V_T ($cm^3 \cdot g^{-1}$)
A120	102	597	0.31	1.05	0.14	0.18	0.63	2.01	0.78	0.78
F120	114	574	0.29	0.99	0.12	0.14	0.55	2.15	0.90	0.64
S120	149	278	0.14	0.92	0.08	0.14	0.36	2.24	1.44	0.25
T120	103	780	0.35	1.00	0.13	0.18	0.66	2.11	0.80	0.77
W120	106	615	0.32	0.99	0.13	0.20	0.66	2.06	0.79	0.78
Z120	103	608	0.30	1.02	0.14	0.19	0.63	1.97	n.d.	n.d.

The textural data obtained for the hybrid catalysts of series 1 are listed in Table 3. As expected, S_{BET} and pore volumes are lower for the catalyst samples than for AC. It is particularly so for samples such as F120 and very especially for S120. Exceptions to the rule are the S_{BET} increase for T120 and the V_T increase for a number of catalyst samples. L_0 only varies slightly for most catalyst samples. However, it markedly increases for A120 and decreases for S120. From data in Table 3 it follows that the effect on porosity is stronger for S120 and weaker for W120. In the case of S120, it does by microporosity > mesoporosity > macroporosity. The reduction of porosity is also high in the three regions of pore sizes for F120. For this sample, however, it is much lower than for S120 and varies by macroporosity > mesoporosity > microporosity. For A120, the porosity decrease is noticeably lower than for F120, regardless of the porosity region. For T120, conversely to S120, microporosity remains nearly unchanged and surface area increases slightly. However, meso- and macroporosity decrease by 13.3 and 14.3%, respectively.

Probably, the most important factor with influence on the porosity of the hybrid catalysts is the diffusion of the catalyst precursor in pores of AC during the impregnation treatment because of the control of the accessibility to the surface active sites of AC and thereby the extent to which the impregnation process occurs, amount of MO precursor supported on AC, and dispersion of the metal catalyst on the surface of AC. If a particular precursor has not access to microporosity of AC, which is where most surface area mainly concentrates for microporous solids, its support on AC would be then greatly mitigated. Diffusion must be mainly dependent on the relative size of the MO precursor and AC pores. For the here used MO precursors, size is a function of whether they are found as a metal cation (Al^{3+}, Fe^{3+}, Sn^{2+}, Zn^{2+}) or anion (WO_4^{2-}) or as a colloidal particle (TiO_2, particle size lower than 44 μm) in the impregnation aqueous system. Under such an

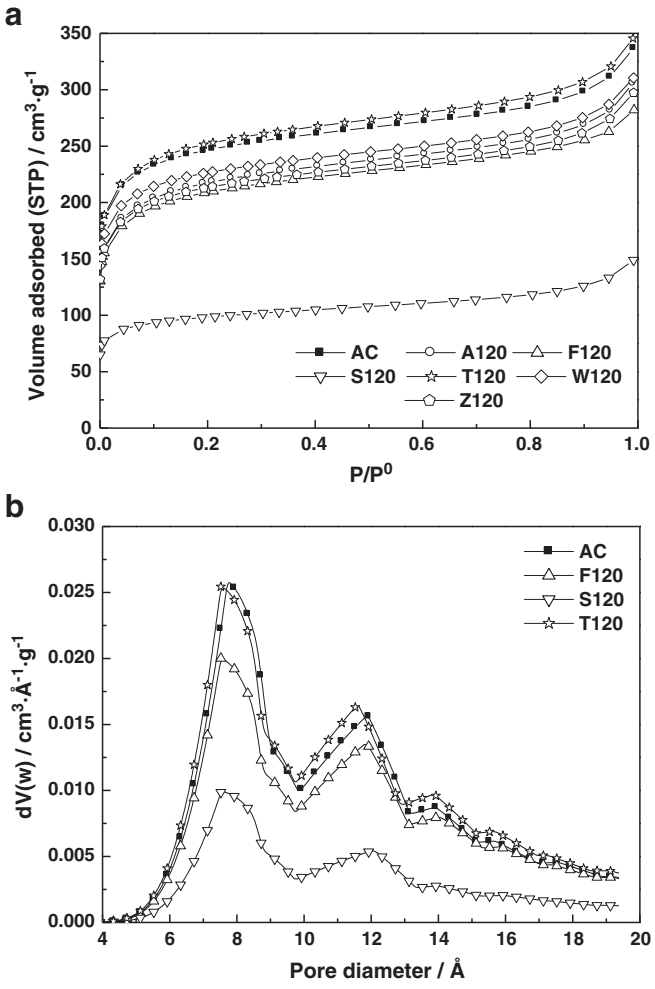

Fig. 3. N_2 adsorption isotherms at −196 °C (a) and micropore size distributions (b) of catalysts of series 1.

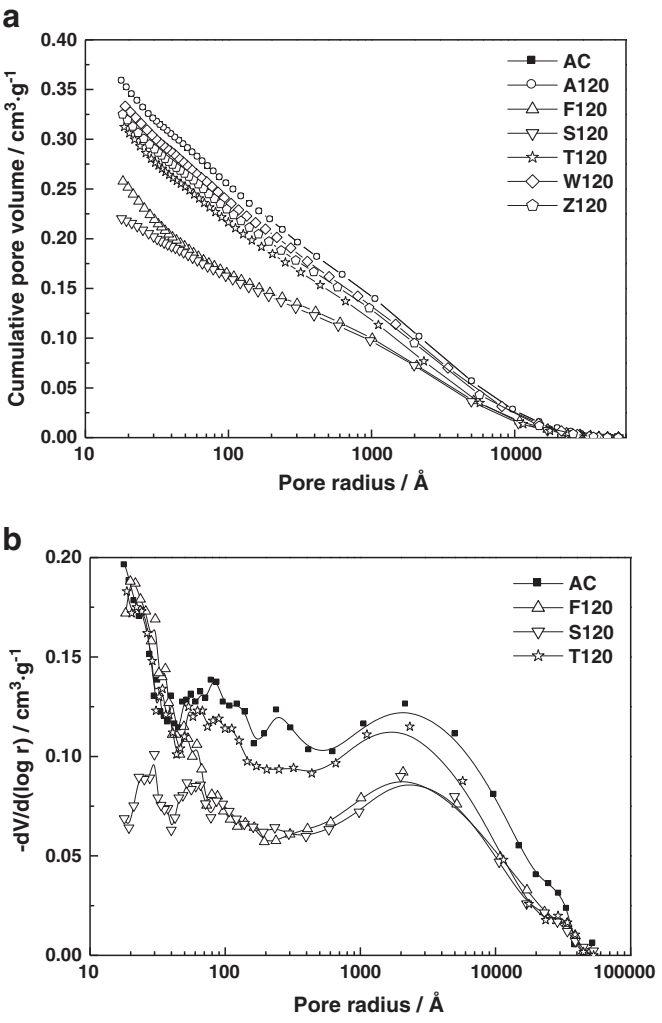

Fig. 4. Cumulative pore volume versus pore radius (a) and meso- and macropore size distributions (b) of catalysts of series 1.

Table 4
Textural data for catalysts of series 2.

Catalyst	Yield (wt.%)	S_{BET} ($m^2 \cdot g^{-1}$)	W_0 ($cm^3 \cdot g^{-1}$)	L_0 (nm)	V_{me} ($cm^3 \cdot g^{-1}$)	V_{ma} ($cm^3 \cdot g^{-1}$)	V_T' ($cm^3 \cdot g^{-1}$)	ρ_{He} ($g \cdot cm^{-3}$)	ρ_{Hg} ($g \cdot cm^{-3}$)	V_T ($cm^3 \cdot g^{-1}$)
A200	93	556	0.27	1.06	0.13	0.16	0.56	2.05	0.91	0.61
F200	94	618	0.29	1.02	0.13	0.14	0.56	2.17	0.90	0.65
S200	96	302	0.15	1.11	0.08	0.13	0.36	2.30	1.06	0.51
T200	96	776	0.35	1.12	0.13	0.19	0.67	2.06	0.97	0.55
W200	96	646	0.32	1.04	0.15	0.17	0.64	2.09	0.70	0.95
Z200	91	651	0.31	0.97	0.18	0.20	0.69	2.07	n.d.	n.d.

assumption, the precursor size (Å) would vary by $TiO_2 > WO_4^{2-} > Sn^{2+}$ (0.93) > Zn^{2+} (0.83) > Fe^{3+} (0.67) Al^{3+}(0.57) [57]. However, it must be taken into account that most metal cations in aqueous solution are found as aquo-complexes, $[M(H_2O)_x]^{n+}$, which hydrolyze by (5)

$$[M(H_2O)_x]^{n+} + yH_2O = [M(H_2O)_{x-y}(OH)_y]^{(n-y)+} + yH_3O^+ \quad (5)$$

giving hydroxo-aquo complexes, $M^{n+}(H_2O)_{x(OH)_y}]^{(n-y)+}$with $[M(H_2O)_{x-y}(OH)_y]^{(n-y)+}$; such that depending on a number of factors including the chemical nature of the metal ion and solution concentration and pH, equilibrium will be more or less displaced toward the left or the right side. For Al^{3+}, Fe^{3+} and Zn^{2+}, the tendency to form hydroxo-aquo complexes at lower pH values varies by $Fe^{3+} > Al^{3+} > Zn^{2+}$ [58]. Replacement of water molecules with hydroxo groups from the coordination sphere of a metal ion-aquo complex will result in a size decrease as the size of the ligand group is smaller for –OH than for H_2O. Depending on concentration, $SnCl_2$ may be also prone to hydrolysis, decomposing to the basic salt Sn(OH)Cl [59]. However, in the presence of activated carbon it undergoes autoxidation at a reaction rate that is dependent on the activation temperature between 350 and 850 °C in the preparation of the carbon [60]. The resulting Sn^{4+} ion in the presence of water is hydrolyzed to a considerable degree, substantially according to reaction (6) [59]

$$Sn^{4+} + 2H_2O = SnO_2 + 4H^+ \quad (6)$$

The tungstate ion (WO_4^{2-}) occurs in water only above pH 8–9. As the pH decreases and hydrogen ions are added to WO_4^{2}, slow polimerization takes place [58] and WO_4^{2-}, HWO_4^- and probably $W_2O_7^{2-}$, $HW_2O_7^-$ and $H_2W_2O_7$ solvated species may be found in aqueous solution [61]. From the WO_4^{2-} ion in aqueous solution, $WO_3 \cdot nH_2O$ (n = 1 or 2) may formed on the surface of AC [62]. Finally, TiO_2 is not soluble in water and therefore the colloidal particles (particle size lower than 44 μm) should remain in suspension in the aqueous medium because of the electrostatic interaction with water molecular dipoles. The size of the TiO_2 precursor may further increase by formation of large aggregates, provided that the surface charges of the particles are not neutralized at the pH of the TiO_2 aqueous suspension.

By taking into account not only the presumable size of the MO precursor in the impregnation system but also the yield of the impregnation process it becomes apparent then that diffusion of the MO precursor in pores of AC is markedly more favourable for Sn(OH)Cl and also, though less, for the Fe^{3+} complexes and that it results in the support of a larger amount of precursor and in a greater microporosity decrease. Furthermore, such precursors should become concentrated in meso- and macropores and these pores are lost as well from AC after the preparation of S120 and F120. Perhaps, the porosity blockage at micropore entrances by a small amount of precursor propitiates its concentration in larger size pores. Consistent with precursor sizes are also the lower detrimental effects on the porous structure for A120 than for F120. TiO_2 should have a more restricted access to AC porosity, which is in line with the textural effects of the TiO_2 support on AC porosity. Likely, microporosity is not affected because of the colloidal size of TiO_2 which would prevent it from entering small size pores of AC. The slight development of mesoporosity, as inferred from the results of N_2 adsorption at −196 °C (notice that a 6.7% decrease is obtained by mercury porosimetry) as a result of the support of TiO_2 on surface of AC may be associated with narrowing of larger size pores due to the accumulation of TiO_2 on pore walls. On the other hand, for W120 it is possible that the yield of the preparation process is over-weighted because of the high density of W (19.3 $g \cdot cm^{-3}$) and its compounds. The opposite applies to A120 as Al is a light metal with a density as low as 2.7 $g \cdot cm^{-3}$. Probably, In comparative terms, the amount of metal present in the hybrid catalyst is smaller and higher for W120 and A120, respectively, than as may be reflect by yield values.

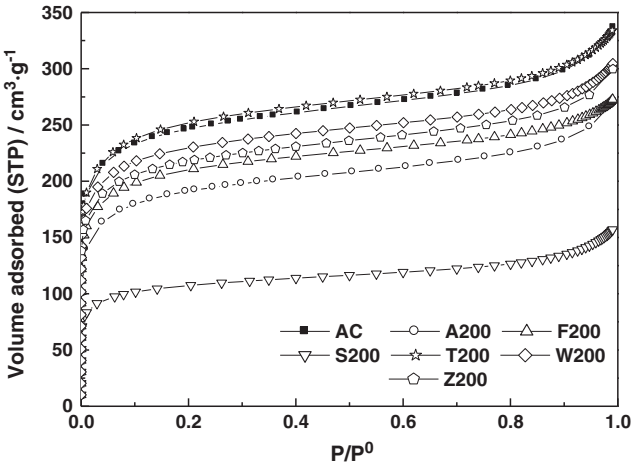

Fig. 5. N_2 adsorption isotherms at −196 °C of the catalysts of series 2.

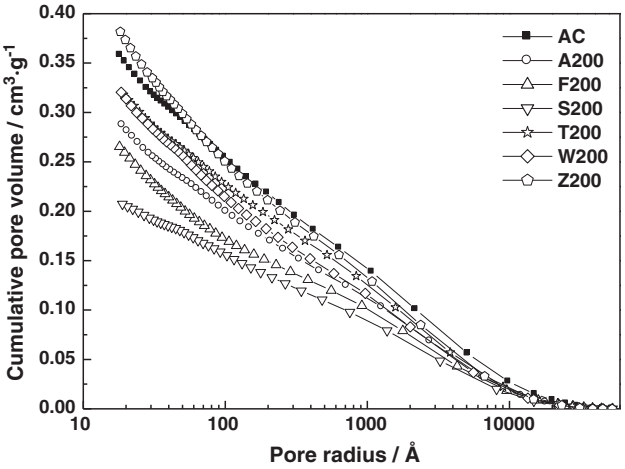

Fig. 6. Cumulative pore volume versus pore radius of the catalysts of series 2.

Table 5
Textural data for catalysts of series 3.

Catalyst	Yield (wt.%)	S_{BET} ($m^2 \cdot g^{-1}$)	W_0 ($cm^3 \cdot g^{-1}$)	L_0 (nm)	V_{me} ($cm^3 \cdot g^{-1}$)	V_{ma} ($cm^3 \cdot g^{-1}$)	V_T' ($cm^3 \cdot g^{-1}$)	ρ_{He} ($g \cdot cm^{-3}$)	ρ_{Hg} ($g \cdot cm^{-3}$)	V_T ($cm^3 \cdot g^{-1}$)
A850	90	759	0.34	1.32	0.14	0.19	0.67	2.07	0.91	0.62
F850	81	694	0.31	1.11	0.17	0.18	0.66	2.19	0.74	0.89
S850	68	680	0.33	1.13	0.16	0.18	0.67	2.25	0.82	0.78
T850	98	847	0.37	1.35	0.14	0.20	0.71	2.08	0.72	0.90
W850	95	741	0.35	1.14	0.15	0.20	0.70	2.13	0.70	0.96
Z850	84	834	0.32	1.08	0.15	0.18	0.65	2.06	n.d.	n.d.

3.3. Series 2

Regarding the hybrid catalysts of series 2, yield (see data in Table 4) varies in the narrow range of 91 wt.% for Z200 and 96 wt.% for S200, T200 and W200. Since yield is 97 wt.% for AC (data in Table 2), it is clear that the subsequent heat treatment of the samples of series 1 at 200 °C only causes a small mass decrease, which is not very different for the various samples of series 2. Nevertheless, it is worth noting that the mass loss is substantially higher for A200, F200 and Z200 than for the rest of the samples. These samples have been prepared from A120, F120 and Z120 (i.e. the products obtained by impregnation of AC with the Al^{3+}, Fe^{3+} and Zn^{2+} ions in the nitrate aqueous solutions) and therefore it is likely that the mass loss produced when they are heat-treated at 200 °C is due to the removal of coordination water of the metal ions remaining in the samples after oven-drying at 120 °C. It is supported by the significantly higher mass loss for Z200 than for A200 and F200 since, as seen above, the aforesaid coordination sphere should be made up of a larger number of water molecules for the Zn^{2+} ion than for the Al^{3+} and Fe^{3+} ions, provided that the coordination number is the same for the three metal ions.

As compared to the isotherms for the catalysts of series 1 in Fig. 3(a), the adsorption isotherms for the hybrid catalysts of series 2 in Fig. 5 display very similar shapes. Accordingly, the heat treatment at 200 °C does not produce significant changes in the micro- and mesopore size distributions of the samples of series 1. A different feature for both bunches of isotherms is the noticeably lower N_2 adsorption for A200, which is worth noting. On the other hand, the curves of mercury intrusion for both series of hybrid catalysts in Figs. 4(a) and 6 reveal that the influence of the chemical nature of the catalyst precursor on the meso- and macropore size distributions is significantly more marked for the hybrid catalysts of series 2.

Likewise, the values of S_{BET} and pore volumes listed in Tables 3 and 4 show that the changes produced in the surface area and porosity of the samples of series 1 as a result of the heat treatment at 200 °C are also generally of little significance. S_{BET} only increases slightly for most samples. For A200, it undergoes a small decrease. W_0 does not undergo significant changes, except for A200. However, L_0 usually increases and is 12.0 and 20.6% higher for T120 and S120, respectively. V_{me} and V_{ma} remain almost unchanged for most samples. In the case of Z200, however, V_{me} increases by 28.6%. V_{ma} decreases by 15% for W200. Finally, it should be mentioned that the values of V_T may be influenced by the density of the metal precursor. As a guide, notice that V_T is much higher than V_T' for W200. However, they are much closer for A200, which is in line with the low Al density.

The aforementioned textural changes must be associated with composition and structural modifications produced in the hybrid catalysts of series 1 after heating at 200 °C. The removal of water from the samples should give rise to porosity development. After the support of the catalyst precursors on AC, surface amorphous pseudo-metal hydroxides, oxy-hydroxides and oxides are likely found in the carbon. A general reaction for the thermal decomposition of metal hydroxides is

$$(OH)_nM(OH)_2 + \Delta \rightarrow (OH)_nMO \quad + H_2O \tag{7}$$

In connection with the removal of water from the samples it should be borne in mind that they were first heat-treated at 200 °C in their preparation and then out-gassed at 120 °C prior to effecting adsorption measurements. Therefore, the presence of water in the samples after out-gassing at 120 °C to some extent will depend on whether the dehydration process at 200 °C is reversible or not. The strongest effect on mesoporosity for Z200 is consistent with the highest mass loss produced in the preparation of this sample, as shown by the yield values collected in Table 4. As an opposite effect to that of the dehydration process, crystallinity may also increase and therefore an increased crystallite size should result in a decreased porosity of the samples. If so, in

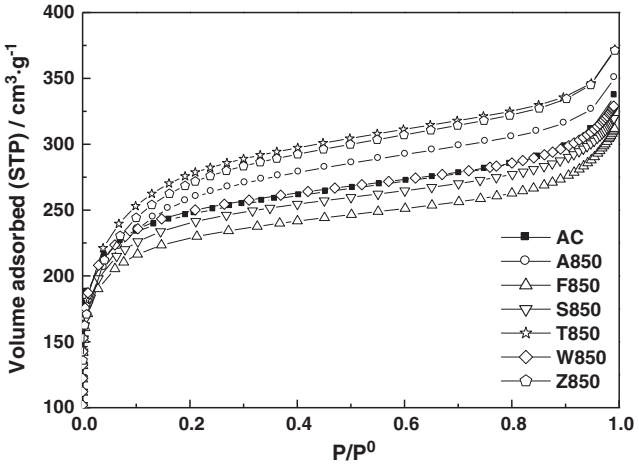

Fig. 7. N_2 adsorption isotherms at −196 °C of the catalysts of series 3.

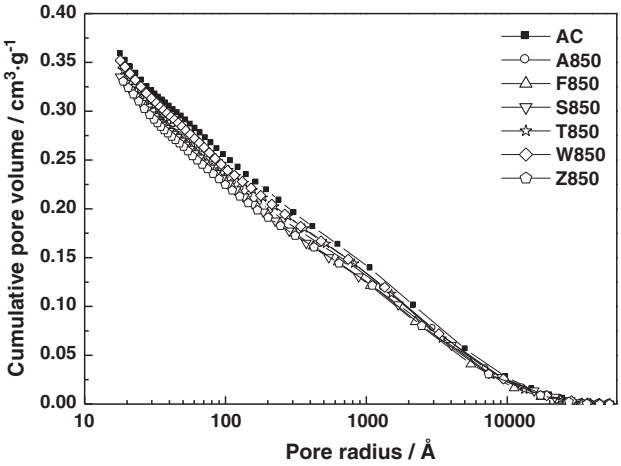

Fig. 8. Cumulative pore volume versus pore radius of the catalysts of series 3.

view of the textural data (Table 4) it seems that both effects on porosity balance for most samples.

3.4. Series 3

For this series of hybrid catalyst samples (data in Table 5) yield varies by the sequence T850 > W850 > A850 > Z850 > F850 > S850 and widely between 98 wt.% for T850 and 68 wt.% for S850. It is low not only for S850 but also for F850 and Z850. The mass loss caused by the heat treatment of the samples up to 850 °C must be due to dehydration and dehydroxilation processes at low temperatures and also to the carbothermic reduction of MOs at higher temperatures. The later reaction gives rise to the formation of gaseous products and of elemental metals which suffer evaporation provided that melting point is below 850 °C. From metallurgy sources concerning the blast furnace performance is well known that various iron oxides are reduced by coke at different temperatures and that elemental iron as a last resort and carbon monoxide are formed. ZnO [63] and SnO_2 [64] are reduced by

$$ZnO + C = Zn + CO \quad (8)$$

$$SnO_2 + C = Sn + CO_2 \quad (9)$$

Reaction (8) is very slow even at 900 °C and reaction (9) occurs above 630 °C. Furthermore, the melting point of Zn is 419.7 °C and of Sn (white) is 231.9 °C Also, Al melts at 660.5 °C. WO_3 transforms to elemental W and metal carbides, giving off CO [26,65]; the melting point of W being however as high as 3407 °C [57].

As compared to the hybrid catalysts of series 1, for the samples of series 3 (see the N_2 adsorption isotherms in Figs. 3(a) and 7) the adsorption of N_2 increases. Furthermore, the isotherm shapes are more similar. It also applies to the curves of mercury intrusion plotted in Fig. 8. Moreover, the estimated values of S_{BET} and pore volumes (data in Table 5) as a rule are higher. This is particularly so for S850 as S_{BET}, W_0, V_{me} and V_T' increase in turn by ≈ 145, 136, 100, and 29%. Then, the porosity development is larger by micropores > mesopores > macropores. For samples other than S850, the increase produced in S_{BET} and pores volumes is much smaller. For F850, it is 21, 7, 42 and 29%, being then higher for V_{me}. In general, L_0 markedly increases. The L_0 increase varies between 6% for Z850 and 35% for T850, being also greater for A850 (26%). Decreased pore volumes are very rarely observed, i.e. only V_{ma} for Z850 and V_T for A850. In brief, from the results obtained in the textural characterization of the hybrid catalysts of series 3 it becomes apparent that by heating at 850 °C porosity develops and the pore size distribution becomes more uniform in the three porosity regions for all catalyst samples. As compared to AC and AC850, a significantly decreased W_0 is observed for a large number of samples. As an exception to the rule, W_0 is 0.37 $cm^3 \cdot g^{-1}$ for T850 and AC850. As shown by the N_2 isotherms (Fig. 7), mesoporosity undergoes an important development for A850, Z850 and T850. However, V_{me} is higher for F850 and S850. Usually, V_{ma} only decreases slightly.

In connection with the textural changes produced by heating at 850 °C it should be first borne in mind that it causes mass loss and thereby porosity increase. Second, the heat treatment at high temperature may also originate composition, structural and textural changes in the carbon support and the supported catalysts with influence on porosity of the hybrid catalysts. In the case of S850 and F850, as two examples, as a result of the reaction of AC with MOs the porosity would be affected by the gasification of carbon atoms and also on account of the formation of smaller atomic/particle size metals as compared to their respective MOs. In the case of catalyst samples such as S850, the evaporation of metal from the melt would render the widening and opening of porosity feasible. These effects on porosity are reflected by the L_0 values obtained for various catalyst samples. Regarding the supported catalyst, the composition and structural changes concern phase transitions, crystallinity, and so on. Finally, contributions to the adsorption of N_2 due to supported catalyst particles have also been reported in the literature for TiO_2 [43].

4. Conclusions

- The AC used as MO support is mainly a microporous carbon. The heat treatment of the carbon at 200 or 850 °C only originates slight changes in the porous texture of the material.
- The yield of the process of preparation of the hybrid catalysts depends on the chemical nature of the MO precursor and on heating conditions. It is very sensitive to the MO precursor when oven-drying at 120 °C and heat-treating at 850 °C. For the resulting series of samples yield varies by S120 ≫ F120 > W120 > T120 > Z120 > A120 and by T850 > W850 > A850 > Z850 > F850 > S850. The mass changes are much stronger for S120 and S850.
- The wet-impregnation of AC and subsequent oven-drying of the resulting products at 120 °C as a rule cause a significant microporosity loss which is higher for F120 and in special for S120. Meso- and macroporosity may also markedly decrease. For S120, porosity is reduced by 61.1, 46.7 and 33.3% for the micro-, meso- and macropores. Conversely, the effects of porosity loss are frequently weaker for W120. For T120, impregnation has a weak beneficial effect on surface area.
- For the AC-MO hybrid catalysts prepared at 200 °C, the MO precursor influences the pore size distribution in the regions of micro- and mesopores. The changes produced in the surface area and pore volumes are generally of little significance. The average size of micropores (L_0) usually increases. The textural effects have been connected with the removal of water and an increased crystallinity because of the heat treatment of the samples at low temperature.
- By heating at 850 °C the pore size distribution becomes more uniform for the hybrid catalysts, AC and AC850. Microporosity pronouncedly increases, the effect being much stronger for the Sn catalyst. However, the micropore volume as a rule is significantly lower for the catalyst samples than for AC and AC850. Mesoporosity develops chiefly for the Sn and Fe catalysts. The textural changes have been associated with mass, composition and structural modifications.
- The method of wet-impregnation of AC with the six MO catalyst precursors in aqueous solution/suspension and oven-drying at 120 °C and subsequent heat treatment of the resulting samples at 200 or 850 °C enables to prepare hybrid catalysts with a different chemical composition, catalyst content, and porous texture.

Acknowledgements

Financial support by Gobierno de Extremadura and European FEDER Funds is gratefully acknowledged. A. Barroso-Bogeat thanks Spanish Ministerio de Educación, Cultura y Deporte for the concession of a FPU grant (AP2010-2574).

References

[1] A. Barroso-Bogeat, C. Fernández-González, M. Alexandre-Franco, V. Gómez-Serrano, Activated carbon as a metal oxide support: A review, in: J.F. Kwiatkowski (Ed.), Activated carbon: classifications, properties and applications, Nova Science Publishers, New York, 2011, pp. 297–318.
[2] L.R. Radovic, C. Sudhakar, Carbon as a catalyst support: Production, properties and applications, in: H. Marsh, E.A. Heintz, F. Rodríguez-Reinoso (Eds.), Introduction to carbon technologies, Universidad de Alicante, Alicante, 1997, pp. 103–165.
[3] L.R. Radovic, F. Rodríguez-Reinoso, Carbon materials in catalysis, in: P.A. Thrower (Ed.), Chemistry and physics of carbon, vol. 25, Marcel Dekker, New York, 1997, pp. 243–258.
[4] F.R. Rodríguez-Reinoso, The role of carbon materials in heterogeneous catalysis, Carbon 36 (1998) 159–175.
[5] H. Marsh, F. Rodríguez-Reinoso, Activated carbon, Elsevier, Oxford, 2006.
[6] P. Serp, J.L. Figueiredo, Carbon materials for catalysis, John Wiley & Sons, Hoboken, NJ, 2009.
[7] H.H. Kung, Transition metal oxides: Surface chemistry and catalysis, Elsevier, Amsterdam, 1989.

[8] V.E. Henrich, P.A. Cox, The surface science of metal oxides, Cambridge University Press, Cambridge, UK, 1994.
[9] C. Noguera, Physics and chemistry at oxide surface, Cambridge University Press, Cambridge, UK, 1996.
[10] M.B. Gawande, R.K. Pandey, R.V. Jayaram, Role of mixed metal oxides in catalysis science-versatile applications in organic synthesis, Catalysis Science & Technology 2 (2012) 1113–1125.
[11] S.D. Jackson, J.S.J. Hargreaves (Eds.), Metal oxide catalysis, Wiley-VCH, Weinheim, 2008.
[12] H.C. Foley, D.S. Lafyatis, R.K. Mariwala, G.D. Sonnichsen, L.D. Brake, Chemical Engineering Science 49 (1994) 4771–4786.
[13] A. Quintanilla, J.A. Casas, J.A. Zazo, A.F. Mohedano, J.J. Rodríguez, Wet air oxidation of phenol at mild conditions with a Fe/activated carbon catalyst, Applied Catalysis, B: Environmental 62 (2006) 115–120.
[14] C.S. Castro, M.C. Guerreiro, L.C.A. Oliveira, M. Gonçalves, A.S. Anastácio, M. Nazzarro, Iron oxide dispersed over activated carbon: Support influence on the oxidation of the model molecule methylene blue, Applied Catalysis, A: General 367 (2009) 53–58.
[15] N. Sobana, M. Swaminathan, Combination effect of ZnO and activated carbon for solar assisted photocatalytic degradation of Direct Blue 53, Solar Energy Materials and Solar Cells 91 (2007) 727–734.
[16] J. Chen, X. Wen, X. Shi, R. Pan, Synthesis of zinc oxide/activated carbon nanocomposites and photodegradation of rhodamine B, Environmental Engineering Science 29 (2012) 392–398.
[17] A. Changsuphan, M.I.B.A. Wahab, N.T.K. Oanh, Removal of benzene by ZnO nanoparticles coated on porous adsorbents in presence of ozone and UV, Chemical Engineering Journal 181–182 (2012) 215–221.
[18] X. Wang, Y. Liu, Z. Hu, Y. Chen, W. Liu, G. Zhao, Degradation of methyl orange by composite photocatalysts nano-TiO_2 immobilized in activated carbons of different porosities, Journal of Hazardous Materials 169 (2009) 1061–1067.
[19] T.S. Jamil, M.Y. Ghaly, N.A. Fathy, T.A. Abd el-halim, L. Österlund, Enhancement of TiO_2 behavior on photocatalytic oxidation of MO dye using TiO_2/AC under visible irradiation and sunlight radiation, Separation and Purification Technology 98 (2012) 270–279.
[20] O.K. Mahadwad, P.A. Parikh, R.V. Jasra, C. Patil, Photocatalytic degradation of reactive black-5 dye using TiO_2-impregneted activated carbon, Environmental Technology 33 (2012) 307–312.
[21] J.S. Choi, T.H. Kim, K.Y. Choo, J.S. Sung, M.B. Saidutta, S.O. Ryu, S.D. Song, B. Ramachandra, Y.W. Rhee, Direct synthesis of phenol from benzene on iron-impregnated activated carbon catalysts, Applied Catalysis, A: General 290 (2005) 1–8.
[22] J.S. Choi, T.H. Kim, K.Y. Choo, J.S. Sung, M.B. Saidutta, S.D. Song, Y.W. Rhee, Transition metals supported on activated carbon as benzene hydroxylation catalysts, Journal of Porous Materials 12 (2005) 301–310.
[23] P. Michorczyk, P. Kustrowski, L. Chmielarz, J. Ogonowski, Influence of the redox properties on activity of iron oxide catalysts in the dehydrogenation of propane with CO_2, Reaction Kinetics and Catalysis Letters 82 (2004) 121–130.
[24] B. Sreedhar, V. Bhaskar, Ch. Sridhar, T. Srinivas, L. Kótai, K. Szentmihályi, Acylation of alcohols and amines with carboxylic acids: A first report catalyzed by iron(III) oxide-containing activated carbon, Journal of Molecular Catalysis A: Chemical 191 (2003) 141–147.
[25] A.F. Pérez-Cardenas, C. Moreno-Castilla, F.J. Maldonado-Hódar, J.L.G. Fierro, Tungsten oxide catalysts supported on activated carbons: effect of tungsten precursor and pretreatment on dispersion, distribution, and surface acidity of catalysts, Journal of Catalysis 217 (2003) 30–37.
[26] M.A. Álvarez-Merino, F. Carrasco-Marín, J.L.G. Fierro, C. Moreno-Castilla, Tungsten catalysts supported on activated carbon: I. Preparation and characterization after their heat treatments in inert atmosphere, Journal of Catalysis 192 (2000) 363–373.
[27] M.A. Álvarez-Merino, F. Carrasco-Marín, C. Moreno-Castilla, Tungsten catalysts supported on activated carbon: II. Skeletal isomerization of 1-butene, Journal of Catalysis 192 (2000) 374–380.
[28] C. Moreno-Castilla, M.A. Álvarez-Merino, F. Carrasco-Marín, Decomposition reactions of methanol and ethanol catalyzed by tungsten oxide supported on activated carbon, Reaction Kinetics and Catalysis Letters 71 (2000) 137–142.
[29] M.A. Álvarez-Merino, M.F. Ribeiro, J.M. Silva, F. Carrasco-Marín, F.J. Maldonado-Hódar, Activated carbon and tungsten oxide supported on activated carbon catalysts for toluene catalytic combustion, Environmental Science and Technology 38 (2004) 4664–4670.
[30] C. Moreno-Castilla, M.A. Álvarez-Merino, F. Carrasco-Marín, J.L.G. Fierro, Tungsten and tungsten carbide supported on activated carbon: Surface structures and performance for ethylene hydrogenation, Langmuir 17 (2001) 1752–1756.
[31] S.E. Iyuke, F.R. Ahmadun, Adsorption and solid catalysed reaction between activated carbon impregnated with SnO_2 and CO at ordinary temperature, Applied Surface Science 187 (2002) 37–44.
[32] F.S. Baltacioglu, B. Gülyüz, A.E. Aksoylu, Z.I. Önsan, Low temperature CO oxidation kinetics over activated carbon supported Pt-SnO_x catalysts, Turkish Journal of Chemistry 31 (2007) 455–464.
[33] P.M. Boorman, R.A. Kydd, T.S. Sorensen, K. Chong, J.M. Lewis, W.S. Bell, A comparison of alumina, carbon and carbon-covered alumina as supports for Ni-Mo-F additives: gas oil hydroprocessing studies, Fuel 71 (1992) 87–93.
[34] F. Liu, S. Xu, Y. Chi, D. Xue, A novel alumina-activated carbon composite supported NiMo catalyst for hydrodesulfurization of dibenzothiophene, Catalysis Communications 12 (2011) 521–524.
[35] P. Ehrburger, Dispersion of small particles on carbon surfaces, Advances in Colloid and Interface Science 21 (1984) 275–302.
[36] J.L. Figeiredo, Funcionalization of porous carbons for catalytic applications, Journal of Materials Chemistry A 1 (2013) 9351–9364.
[37] W. Ma, E.L. Kugler, D.B. Dadyburjor, Effect of properties of various activated-carbon supports and supported Fe-Mo-Cu-K catalysts on metal precursor distribution, metal reduction, and Fisher-Tropsch synthesis, Energy and Fuels 24 (2010) 4099–4110.
[38] M.C. Román-Martínez, D. Cazorla-Amorós, A. Linares-Solano, C. Salinas- Martínez de Lecea, Metal-support interaction in Pt/C catalysts. Influence of the support surface chemistry and the metal precursor, Carbon 33 (1995) 3–12.
[39] H.H. Tseng, M.Y. Wey, Study of SO_2 adsorption and thermal regeneration over activated carbon-supported copper oxide catalysts, Carbon 42 (2004) 2269–2278.
[40] J.A. Schwarz, C. Contescu, A. Contescu, Methods of preparation of catalytic materials, Chemical Reviews 95 (1995) 477–510.
[41] A. Kahn, TiO_2 coated activated carbon for water recovery, Journal of Undergraduate Research 3 (June 2002).
[42] A.H. El-Sheikh, A.P. Newman, H. Al-Daffaee, S. Phull, N. Cresswell, S. York, Deposition of anatase on the surface of activated carbon, Surface and Coatings Technology 187 (2004) 284–292.
[43] Y. Ao, J. Xu, X. Shen, D. Fu, C. Yuan, Magnetically separable composite photocatalyst with enhanced photocatalytic activity, Journal of Hazardous Materials 160 (2008) 295–300.
[44] S.J. Gregg, K.S.W. Sing, Adsorption, surface area and porosity, Academic Press, London, 1982.
[45] G. Horváth, K. Kawazoe, Method for the calculation of effective pore size distribution in molecular sieve carbon, Journal of Chemical Engineering of Japan 16 (1983) 470–475.
[46] M.M. Dubinin, Physical adsorption of gases and vapors in micropores, in: J.F. Danielli, M.D. Rosenberg, D.A. Cadenhead (Eds.), Progress in Surface and Membrane Science, vol. 9, Academic Press, New York, 1975, pp. 1–70.
[47] T.A. Centeno, F. Stoeckli, The assessment of surface areas in porous carbons by two model-independent techniques, the DR equation and DFT, Carbon 48 (2010) 2478–2486.
[48] S. Brunauer, P.H. Emmett, T. Teller, Adsorption of gases in multimolecular layers, Journal of the American Chemical Society 60 (1938) 309–319.
[49] M. Smisek, S. Cerny, Active carbon, Manufacture, properties and applications, , Elsevier, Amsterdam, 1970.
[50] S. Brunauer, L. Deming, W. Deming, E. Teller, On the theory of the van der Waals adsorption of gases, Journal of the American Chemical Society 62 (1940) 1723–1732.
[51] M. Olivares-Marín, C. Fernández-González, A. Macías-García, V. Gómez-Serrano, Preparation of activated carbon from cherry stones by physical activation in air. Influence of the chemical carbonisation with H_2SO_4, Journal of Analytical and Applied Pyrolysis 94 (2012) 131–137.
[52] J.W. Neely, Characterization of polymer carbons derived from porous sulfonated polystyrene, Carbon 19 (1981) 27–36.
[53] V. Gómez-Serrano, J. Pastor-Villegas, C.J. Duran-Valle, Heat treatment of rockrose char in air. Effect on surface chemistry and porous texture, Carbon 34 (1996) 533–538.
[54] M. Ruiz-Fernández, M. Alexandre-Franco, C. Fernández-González, V. Gómez-Serrano, Development of activated carbon from vine shoots by physical and chemical activation methods. Some insight into activation mechanisms, Adsorption 17 (2011) 621–629.
[55] K.J. Master, B. McEnaney, The development of structure and microporosity in cellulose carbon, Carbon 22 (1984) 595-560.
[56] P.N. Cheremisinoff, F. Ellerbusch (Eds.), Carbon adsorption handbook, Ann Arbor Science, Ann Arbor, MI, 1980.
[57] J. Emsley, The Elements, Clarendon Press, Oxford, 1989.
[58] C.F. Baes Jr., R.E. Mesmer, The hydrolysis of cations, John Wiley & Sons, New York, 1976.
[59] H. Remi, Treatise of inorganic chemistry, vol. 1, Elsevier, Amsterdam, 1956.
[60] E.C. Larsen, J.H. Walton, Activated carbon as a catalyst in certain oxidation-reduction reactions, Journal of Physical Chemistry 44 (1940) 70–87.
[61] T. Barré, L. Arurault, F.X. Sauvage, Chemical behavior of tungstate solutions. Part 1. A spectroscopic survey of species involved, Spectrochimica Acta, Part A 61 (2005) 551–557.
[62] F.A. Cotton, G. Wilkinson, Química Inorgánica Avanzada, Limusa, México, 1986.
[63] B.S. Kim, J.M. Yoo, J.T. Park, J.C. Lee, A kinetic study of the carbothermic reduction of zinc oxide with various additives, Materials Transactions, JIM 47 (2006) 2421–2426.
[64] R. Padilla, The reduction of cassiterite with carbon, (Ph. D. Thesis) University of Utah, 1977.
[65] G.A. Swift, R. Koc, Tungsten powder from carbon coated WO_3 precursors, Journal of Materials Science 36 (2001) 803–806.